Research Article

Detecting Changes in the Mean of an Integration and Fractionally Integrated MA Process on Double Modified EWMA Control Chart

Julalak Neammai, Yupaporn Areepong* and Saowanit Sukparungsee
Department of Applied Statistics, Faculty of Applied Science, King Mongkut's University of Technology North Bangkok, Bangkok, Thailand

* Corresponding author. E-mail: yupaporn.a@sci.kmutnb.ac.th DOI: 10.14416/j.asep.2025.07.011
Received: 1 April 2025; Revised: 13 May 2025; Accepted: 10 June 2025; Published online: 23 July 2025

Abstract
Stock market behavior is inherently volatile and sensitive to external influences, making effective monitoring tools essential for detecting shifts in financial time series. This study proposes a Double Modified Exponentially Weighted Moving Average (DMEWMA) control chart designed to improve the detection of small mean shifts in autocorrelated stock data modeled by Integrated Moving Average (IMA) and Fractionally Integrated Moving Average (FIMA) processes with exponential white noise. The Average Run Length (ARL) performance of the proposed chart is analytically derived using both an exact formula based on Fredholm integral equations and a Numerical Integral Equation (NIE) technique. The simulations confirm the accuracy of the analytical results. Comparative analysis demonstrates that the DMEWMA chart outperforms the Modified EWMA (MEWMA) chart across various shift magnitudes, exhibiting lower ARL_1, Relative Median Index (RMI), and Average Expected Quadratic Loss (AEQL) values. Real-world applications using Thai stock data further validate the practical utility of the proposed method, highlighting its superior sensitivity in detecting subtle process changes.

Keywords: Double modified EWMA control chart, Explicit formula, Fractionally integrated moving average, Integrated moving average, Numerical integral equations

1 Introduction

Statistical process control (SPC) is a fundamental method for monitoring and improving the quality and stability of processes across industries. The control chart, established by Shewhart [1], is one of the most extensively used tools in SPC. Control charts are critical for distinguishing between common cause variations, which are inherent in a process, and special cause variations, which indicate the presence of an assignable element that requires corrective action [2]. By continuously analyzing process data, control charts allow organizations to detect variations early, minimize defects, and ensure consistent product quality [3]. The two main types of control charts are attribute control charts and variable control charts. For continuous data like temperature, weight, or pressure, variable control charts like the $\bar{X}$-R, $\bar{X}$-S, and exponentially weighted moving average (EWMA) charts are utilized [2]. On the other hand, attribute control charts, such as the p-chart, np-chart, c-chart, and u-chart, are used to represent categorical data, including the percentage of non-conforming products or the quantity of defective items in a batch [4]. The type of data being evaluated and the process's characteristics determine which control chart is best. Control chart implementation is essential for improving operational efficiency and guaranteeing process stability. In order to make data-driven decisions that lower variability and boost performance, organizations use these charts to spot trends, changes, and out-of-control situations [2].

The concept of control charts for monitoring process stability was first introduced by Shewhart [1], laying the groundwork for modern statistical process control techniques. While the Shewhart control chart remains effective for detecting large shifts in process behavior, its reliance on the most recent observation

limits its ability to identify smaller, more subtle deviations [2]. To address this limitation, memory-based control charts, such as the cumulative sum (CUSUM) [5] and exponentially weighted moving average (EWMA) charts [6], were developed. By incorporating historical data, these charts enhance the sensitivity to small-to-moderate shifts in process parameters, providing a more comprehensive approach to process monitoring [7]. Despite their effectiveness, traditional EWMA charts may still exhibit limitations in responsiveness to subtle process variations. To enhance performance, the Modified Exponentially Weighted Moving Average (MEWMA) and the Double Modified Exponentially Weighted Moving Average (DMEWMA) control charts have been introduced. The MEWMA chart [8] improves upon the classical EWMA by adjusting the smoothing parameter to better adapt to different types of shifts. The DMEWMA control chart, on the other hand, further extends the EWMA framework by incorporating an additional smoothing parameter. The key difference is that the DMEWMA chart applies two levels of exponential smoothing, allowing it to respond more effectively to subtle process variations [9]. These modifications make both MEWMA and DMEWMA more sensitive to subtle changes in process behavior compared to traditional EWMA charts. In addition to DMEWMA, other advanced monitoring techniques, such as the generalized likelihood ratio (GLR) and adaptive EWMA charts, have been developed to further refine statistical process control in various applications [10].

The assumption that observations are independent and identically distributed (i.i.d.) is a major restriction of memory-based control charts, as it may not always be valid in real applications. In many manufacturing processes and other domains, observations might show autocorrelation, which occurs when the current data point is associated with previous observations [2]. Autocorrelation in data has been extensively studied using various time series models, including autoregressive (AR), moving average (MA), autoregressive moving average (ARMA), autoregressive integrated moving average (ARIMA), autoregressive fractionally integrated moving average (ARFIMA) models, which are commonly used to model time-dependent processes [11].

The average run length (ARL) is an important metric for evaluating control chart performance since it represents the average number of observations required to identify a signal (showing a process shift) [2]. The ARL evaluates the sensitivity of a control chart, with a shorter ARL indicating faster shift detection. There are two main approaches for estimating the ARL: Monte Carlo simulation and numerical integral equation (NIE). To determine the frequency of a signal and replicate the process, a Monte Carlo simulation generates random samples. It is frequently used to assess autocorrelated data and intricate control charts [12]. However, NIE is computationally more efficient and models the process distribution by solving integral equations, particularly when large amounts of data or analytical solutions are needed [13]. Both approaches are useful resources for examining the performance of control charts, and each has benefits based on the processing demands and data complexity. An explicit formula for the exact ARL can be derived from certain types of control charts, particularly when the distribution of the control statistic is known under both in-control and out-of-control scenarios. As the determination of ARL for MA processes has been extensively studied [14]–[17], including its application to the DMEWMA control chart [18], this study extends the analysis of the DMEWMA chart to IMA and FIMA processes. These processes have previously been examined in the context of the MEWMA control chart [19], and their integration into the DMEWMA framework aims to enhance process monitoring capabilities in more complex time-series environments. The primary goal of this research is to propose an exact formula for detecting shifts in the mean of IMA and FIMA processes with exponential white noise, using analytical integral equations (IE) within the context of the DMEWMA control chart.

2 Materials and Methods

2.1 *Statistical methods*

2.1.1 Double modified EWMA control chart, DMEWMA

Let Z_t be the sequence of a generalized long-memory process with exponential white noise. The Double Moving Exponentially Weighted Moving Average control chart is an advanced statistical process monitoring tool used to detect small shifts in a process mean or variance over time. It is an extension of the Modified Exponentially Weighted Moving Average (MEWMA) control chart, incorporating a second level of smoothing to enhance sensitivity to small process

changes. The DMEWMA statistic is defined by Equation (1):

$$Z_t^{(2)} = (1-\lambda_2) Z_{t-1}^{(2)} + \lambda_2 Z_t^{(1)} + \kappa_2 \left(Z_t^{(1)} - Z_{t-1}^{(1)} \right) \quad (1)$$

where $Z_t^{(1)} = (1-\lambda_1) Z_{t-1}^{(1)} + \lambda_1 X_t + \kappa_1 \left(X_t - X_{t-1} \right)$ is the MEWMA statistic, X_t is the process, λ_1, λ_2 are the smoothing parameter satisfying $\lambda_1, \lambda_2 \in (0,1]$. In general, the smoothing constant close to one is ideal for detecting large shifts, while a smaller $\lambda_1, \lambda_2 \in [0.05, 0.25]$ value is recommended for detecting small shifts [20], κ_1, κ_2 are constants. The initial values of $Z_0^{(2)} = Z_0^{(1)} = X_0 = \mu$. The lower control limit (LCL) and upper control limit (UCL) of the DMEWMA control chart can be calculated as follows:

$$\text{control limit} = \begin{cases} \mu - L\sigma\sqrt{\sigma_Z^2}, & LCL \\ \mu + L\sigma\sqrt{\sigma_Z^2}, & UCL \end{cases}$$

where μ and σ are average and standard deviation of the process, L is the coefficient of the control limit, and σ_Z^2 is the variance of the control chart.

The practical success of a DMEWMA chart in monitoring real-world processes depends heavily on the appropriate choice of its smoothing parameters. These parameters—denoted as λ_1 and λ_2 —control the weight applied to past data in the two-stage exponential averaging structure. Their selection should align with the magnitude of shifts the chart is expected to detect:

Small shifts ($\leq 0.2\sigma$): Lower values of λ, such as $\lambda_1 = 0.05, \lambda_2 = 0.1$, improve sensitivity by giving more weight to recent data.

Moderate shifts ($0.2–0.5\sigma$): Balanced values (e.g., $\lambda_1 = 0.1 - 0.15, \lambda_2 = 0.15 - 0.2$) offer a trade-off between responsiveness and robustness.

Large shifts ($\geq 0.5\sigma$)**:** Higher smoothing values (e.g., $\lambda_1 = 0.2 - 0.25, \lambda_2 = 0.25 - 0.3$) reduce noise and false alarms in processes with significant variations.

The table below summarizes these guidelines. All configurations were validated through simulation to ensure the in-control Average Run Length (ARL_0) remains approximately 370, providing consistent baseline performance.

Table 1: Recommended smoothing parameter settings for DMEWMA chart.

Expected Shift Size	Sensitivity Target	Recommended	
		λ_1	λ_2
≤ 0.2	High (small shift detection)	0.05	0.10
0.2–0.5	Balanced	0.10–0.15	015–0.20
≥ 0.5	Low false alarm	0.20–0.25	0.25–0.30

Note: These values are derived based on analytical ARL results and validated via simulation. Users may fine-tune based on their domain-specific process characteristics.

2.1.2 The integrated moving average model, IMA

The integrated moving average model (*IMA*(*d*,*q*)) is a specific case of the ARIMA model where there is no autoregressive component ($p = 0$) and it focuses solely on the integration ($d > 0$) and moving average ($q > 0$) components i.e., *ARIMA*(0,*d*,*q*) = *IMA*(*d*,*q*). It is employed for time series that need to be differenced in order to eliminate seasonality or trends, and the residuals are then modeled using a moving average component. The general expression for *IMA*(*d*,*q*) processes $\{I_t\}$ may be defined by the Equations (2).

$$(1-B)^d I_t = \theta_0 + \Theta(B)\varepsilon_t, \quad (2)$$

where $\Theta(B) = 1 - \theta_1 B - \theta_2 B^2 - ... - \theta_q B^q$ is moving-average operators,backward shift operator; is the B i.e., $B^q \varepsilon_t = \varepsilon_{t-q}$ and $(1-B)^d$ is the differencing operator given by the binomial expansion [21] $(1-B)^d = \sum_{j=0}^{\infty} \frac{\Gamma(j-d)}{\Gamma(j+1)\Gamma(-d)} B^j$ where $\Gamma(\cdot)$ is the gamma function.

For small values of B the first few terms in the expansion is:

$$(1-B)^d I_t = I_t - dI_{t-1} + \frac{d(d-1)}{2!} I_{t-2} - \frac{d(d-1)(d-2)}{3!} I_{t-3} + ... \quad (3)$$

Consequently, the IMA model can be elegantly reformulated using Equations (2) and (3):

$$I_t = \theta_0 + \left(\varepsilon_t - \theta_1\varepsilon_{t-1} - \theta_2\varepsilon_{t-2} - \ldots - \theta_q\varepsilon_{t-q}\right) + \left(dI_{t-1} - \frac{d(d-1)}{2!}I_{t-2} + \frac{d(d-1)(d-2)}{3!}I_{t-3} - \ldots\right) \quad (4)$$

where $-1 < \theta_i < 1$ are coefficient of the MA model, θ_0 is the mean of the process, $\{\varepsilon_t\}$ is white noise sequence with mean $1/\nu$ and variance $1/\nu^2; Exp(\nu)$ and the initial values of $I_{t-1}, I_{t-2}, I_{t-3}, \ldots$ are equal 1.

2.1.3 The fractionally integrated moving average model, FIMA

The fractionally integrated moving average model *(FIMA(d,q))* is an extension of the *IMA*(*d*,*q*) model, allowing for fractional differencing instead of integer differencing, i.e.; $-\frac{1}{2} \le d = \frac{m}{n} \le \frac{1}{2}$. The *FIMA*(*d*,*q*) long-memory process follows the same Equation (4) as the *IMA*(*d*,*q*) model, with the key distinction that d is replaced by $d = m/n$, allowing for fractional differencing.

$$FI_t = \theta_0 + \left(\varepsilon_t - \theta_1\varepsilon_{t-1} - \theta_2\varepsilon_{t-2} - \ldots - \theta_q\varepsilon_{t-q}\right) + \left(\frac{m}{n}FI_{t-1} - \frac{\frac{m}{n}\left(\frac{m}{n}-1\right)}{2!}FI_{t-2} + \frac{\frac{m}{n}\left(\frac{m}{n}-1\right)\left(\frac{m}{n}-2\right)}{3!}FI_{t-3} - \ldots\right) \quad (5)$$

where *m* and *n* are constant and *m* < *n*.

2.1.4 The design of the IMA and FIMA - DMEWMA scheme

Equation (1) can be modified by substituting the *IMA*(*d*,*q*) process (X_t) from Equation (4). Thus, the DMEWMA statistic in Equation (1) is calculated as

$$Z_t^{(2)} = (1-\lambda_2)Z_{t-1}^{(2)} + (\lambda_2 - \lambda_1\lambda_2 - \lambda_1\kappa_2)Z_{t-1}^{(1)} + (\lambda_1\lambda_2 + \kappa_1\lambda_2 + \lambda_1\kappa_2 + \kappa_1\kappa_2)X_t - (\kappa_1\lambda_2 + \kappa_1\kappa_2)X_{t-1}$$

Plug in the *IMA*(*d*,*q*) process in to $Z_t^{(2)}$;

$$Z_t^{(2)} = (1-\lambda_2)Z_{t-1}^{(2)} + (\lambda_2 - \lambda_1\lambda_2 - \lambda_1\kappa_2)Z_{t-1}^{(1)} + (\lambda_1\lambda_2 + \kappa_1\lambda_2 + \lambda_1\kappa_2 + \kappa_1\kappa_2)\varepsilon_t + (\lambda_1\lambda_2 + \kappa_1\lambda_2 + \lambda_1\kappa_2 + \kappa_1\kappa_2)\left(\theta_0 - \left(\theta_1\varepsilon_{t-1} + \theta_2\varepsilon_{t-2} + \ldots + \theta_q\varepsilon_{t-q}\right) + \left(dI_{t-1} - \frac{d(d-1)}{2!}I_{t-2} + \frac{d(d-1)(d-2)}{3!}I_{t-3} - \ldots\right)\right) - (\kappa_1\lambda_2 + \kappa_1\kappa_2)X_{t-1}$$

Setting $Z_{t-1}^{(2)} = \zeta$. Then, the proposed DMEWMA statistic becomes

$$Z_t^{(2)} = (1-\lambda_2)\zeta + (\lambda_2 - \lambda_1\lambda_2 - \lambda_1\kappa_2)Z_{t-1}^{(1)} + (\lambda_1\lambda_2 + \kappa_1\lambda_2 + \lambda_1\kappa_2 + \kappa_1\kappa_2)\varepsilon_t + (\lambda_1\lambda_2 + \kappa_1\lambda_2 + \lambda_1\kappa_2 + \kappa_1\kappa_2)\left(\theta_0 - \left(\theta_1\varepsilon_{t-1} + \theta_2\varepsilon_{t-2} + \ldots + \theta_q\varepsilon_{t-q}\right) + \left(dI_{t-1} - \frac{d(d-1)}{2!}I_{t-2} + \frac{d(d-1)(d-2)}{3!}I_{t-3} - \ldots\right)\right) - (\kappa_1\lambda_2 + \kappa_1\kappa_2)X_{t-1}$$

The stopping time, denoted as τ, is a random variable representing the time (or number of observations) until the DMEWMA statistic first exceeds the control limits, signaling a process change. Mathematically, it can be defined as:

$$\tau_{L_1,U_1} = \inf\left\{t > 0; Z_t^{(2)} \notin (L_1, U_1)\right\},$$

where L_1 is the lower control limit, and U_1 is the upper control limit. For the in-control process, the interval $Z_t^{(2)}$ between the lower and upper control limits can be written as $L_1 < \varepsilon_t < U_1$.

This can be restated for ε_t on the interval as follows:

$$\frac{L_1 - (1-\lambda_2)\zeta - (\lambda_2 - \lambda_1\lambda_2 - \lambda_1\kappa_2)Z_{t-1}^{(1)} + (\kappa_1\lambda_2 + \kappa_1\kappa_2)X_{t-1} - (\lambda_1\lambda_2 + \kappa_1\lambda_2 + \lambda_1\kappa_2 + \kappa_1\kappa_2)\Delta}{\lambda_1\lambda_2 + \kappa_1\lambda_2 + \lambda_1\kappa_2 + \kappa_1\kappa_2} < \varepsilon_t <$$

$$\frac{U_1 - (1-\lambda_2)\zeta - (\lambda_2 - \lambda_1\lambda_2 - \lambda_1\kappa_2)Z_{t-1}^{(1)} + (\kappa_1\lambda_2 + \kappa_1\kappa_2)X_{t-1} - (\lambda_1\lambda_2 + \kappa_1\lambda_2 + \lambda_1\kappa_2 + \kappa_1\kappa_2)\Delta}{\lambda_1\lambda_2 + \kappa_1\lambda_2 + \lambda_1\kappa_2 + \kappa_1\kappa_2}$$

where

$$\Delta = \begin{pmatrix} \theta_0 - \left(\theta_1\varepsilon_{t-1} + \theta_2\varepsilon_{t-2} + ... + \theta_q\varepsilon_{t-q}\right) \\ + \left(dI_{t-1} - \frac{d(d-1)}{2!} I_{t-2} + \frac{d(d-1)(d-2)}{3!} I_{t-3} - ... \right) \end{pmatrix}.$$

The DMEWMA statistic on FIMA can be modified by substituting the *FIMA*(*d*,*q*) process (X_t) from Equation (5). Because the FIMA process is an extension of the IMA process, in which d can be a fraction ($d = m/n$) the interval $Z_t^{(2)}$ between the lower and upper control limits can be rewritten as indicated.

$$\frac{\begin{matrix} L_2 - (1-\lambda_2)\zeta - (\lambda_2 - \lambda_1\lambda_2 - \lambda_1\kappa_2) Z_{t-1}^{(1)} \\ + (\kappa_1\lambda_2 + \kappa_1\kappa_2) X_{t-1} - (\lambda_1\lambda_2 + \kappa_1\lambda_2 + \lambda_1\kappa_2 + \kappa_1\kappa_2)\Omega \end{matrix}}{\lambda_1\lambda_2 + \kappa_1\lambda_2 + \lambda_1\kappa_2 + \kappa_1\kappa_2} < \varepsilon_t$$

$$\frac{\begin{matrix} U_2 - (1-\lambda_2)\zeta - (\lambda_2 - \lambda_1\lambda_2 - \lambda_1\kappa_2) Z_{t-1}^{(1)} + (\kappa_1\lambda_2 + \kappa_1\kappa_2) X_{t-1} \\ - (\lambda_1\lambda_2 + \kappa_1\lambda_2 + \lambda_1\kappa_2 + \kappa_1\kappa_2)\Omega \end{matrix}}{\lambda_1\lambda_2 + \kappa_1\lambda_2 + \lambda_1\kappa_2 + \kappa_1\kappa_2}$$

where

$$\Omega = \begin{pmatrix} \theta_0 - \left(\theta_1\varepsilon_{t-1} + \theta_2\varepsilon_{t-2} + ... + \theta_q\varepsilon_{t-q}\right) \\ + \left(\frac{m}{n} FI_{t-1} - \frac{\frac{m}{n}\left(\frac{m}{n}-1\right)}{2!} FI_{t-2} + \frac{\frac{m}{n}\left(\frac{m}{n}-1\right)\left(\frac{m}{n}-2\right)}{3!} FI_{t-3} - ... \right) \end{pmatrix}$$

and L_2 is the lower control limit, and U_2 is the upper control limit of the FIMA process.

2.2 *Method of calculating a control chart*

Let $\varepsilon_t;\ t = 1,2,3,...$ be the sequence of continuous that is independent and identically distributed random variables from an exponential distribution with parameter ν. The stochastic features of the stopping time in relation to the DMEWMA control chart are critical for understanding its performance in detecting process alterations. The stopping time is the point when the control chart indicates an out-of-control condition. The Average Run Length (ARL) can be rigorously defined using expectation notation while accounting for a fixed change point *i*. When considering a process where a shift occurs at a specific time i, we define the ARL more precisely as: $ARL(i) = E_i[t]$ when $E_i[.]$ is the expectation operator conditioned on a fixed change point *i*. This enables us to separate ARL into two main conditions:

In-Control ARL (ARL_0) is the ARL when the process is stable (before any shift occurs). It is defined as: $ARL_0 = E_\infty(\tau_{LB,UB})$. An appropriate control chart should include a large ARL. Out-of-Control ARL (ARL_1) with change point i. If a shift occurs at time i, then the ARL depends on when the shift is detected: $ARL_1 = E_1(\tau_{LB,UB} \mid \tau_{LB,UB} \geq i)$. An appropriate control chart should include a small ARL.

2.2.1 The IMA - DMEWMA Exact Formula based on Fredholm Integral Equation

Let $I(\zeta)$ be the analytical ARL used to identify shifts in the $IMA(d,q)$ process with exponential white noise $(\varepsilon_t \sim Exp(\nu))$ running on the DMEWMA control chart when the initial value of $Z_{t-1}^{(2)}$ is ξ defined as

$$I(\xi) = 1 + \int_{L_1}^{U_1} I \begin{pmatrix} (1-\lambda_2)\zeta + (\lambda_2 - \lambda_1\lambda_2 - \lambda_1\kappa_2) Z_{t-1}^{(1)} \\ - (\kappa_1\lambda_2 + \kappa_1\kappa_2) X_{t-1} \\ + (\lambda_1\lambda_2 + \kappa_1\lambda_2 + \lambda_1\kappa_2 + \kappa_1\kappa_2)\Delta \\ + (\lambda_1\lambda_2 + \kappa_1\lambda_2 + \lambda_1\kappa_2 + \kappa_1\kappa_2)\omega \end{pmatrix} \cdot f(\omega) d\omega$$

The integral equation can be found by changing the integral variables as follows:

Let

$$\begin{aligned} s = {} & (1-\lambda_2)\zeta + (\lambda_2 - \lambda_1\lambda_2 - \lambda_1\kappa_2) Z_{t-1}^{(1)} - (\kappa_1\lambda_2 + \kappa_1\kappa_2) X_{t-1} \\ & + (\lambda_1\lambda_2 + \kappa_1\lambda_2 + \lambda_1\kappa_2 + \kappa_1\kappa_2)\Delta \\ & + (\lambda_1\lambda_2 + \kappa_1\lambda_2 + \lambda_1\kappa_2 + \kappa_1\kappa_2)\omega \end{aligned}$$

Then,

$$\omega = \frac{\begin{matrix} s - (1-\lambda_2)\zeta - (\lambda_2 - \lambda_1\lambda_2 - \lambda_1\kappa_2) Z_{t-1}^{(1)} \\ + (\kappa_1\lambda_2 + \kappa_1\kappa_2) X_{t-1} - (\lambda_1\lambda_2 + \kappa_1\lambda_2 + \lambda_1\kappa_2 + \kappa_1\kappa_2)\Delta \end{matrix}}{(\lambda_1\lambda_2 + \kappa_1\lambda_2 + \lambda_1\kappa_2 + \kappa_1\kappa_2)}$$

and $d\omega = \frac{1}{\lambda_1\lambda_2 + \kappa_1\lambda_2 + \lambda_1\kappa_2 + \kappa_1\kappa_2} ds$

The integral equations can be obtained by altering the integral variable as

$$I(\zeta)=1+\frac{1}{\lambda_1\lambda_2+\kappa_1\lambda_2+\lambda_1\kappa_2+\kappa_1\kappa_2}\times \int_{L_1}^{U_1} I(s)\, f\left(\begin{array}{l} s-(1-\lambda_2)\zeta-(\lambda_2-\lambda_1\lambda_2-\lambda_1\kappa_2)Z_{t-1}^{(1)} \\ +(\kappa_1\lambda_2+\kappa_1\kappa_2)X_{t-1} \\ \dfrac{-(\lambda_1\lambda_2+\kappa_1\lambda_2+\lambda_1\kappa_2+\kappa_1\kappa_2)\Delta}{(\lambda_1\lambda_2+\kappa_1\lambda_2+\lambda_1\kappa_2+\kappa_1\kappa_2)} \end{array}\right) ds$$

Since the function of $\varepsilon_t \sim Exp(\nu)$ is $f(x)=\frac{1}{\nu}\exp\left(\frac{-x}{\nu}\right)$, then $I(\zeta)$ can be rewritten as:

$$I(\xi)=1+\frac{1}{\nu(\lambda_1\lambda_2+\kappa_1\lambda_2+\lambda_1\kappa_2+\kappa_1\kappa_2)}\times \int_{L_1}^{U_1} I(s)\exp\left(\frac{-\left(\begin{array}{l} s-(1-\lambda_2)\zeta-(\lambda_2-\lambda_1\lambda_2-\lambda_1\kappa_2)Z_{t-1}^{(1)} \\ +(\kappa_1\lambda_2+\kappa_1\kappa_2)X_{t-1} \\ -(\lambda_1\lambda_2+\kappa_1\lambda_2+\lambda_1\kappa_2+\kappa_1\kappa_2)\Delta \end{array}\right)}{\nu(\lambda_1\lambda_2+\kappa_1\lambda_2+\lambda_1\kappa_2+\kappa_1\kappa_2)}\right) ds \quad (6)$$

Equation (6) was evaluated using Banach's fixed-point theorem to ensure its existence and uniqueness.

To improve the tractability of Equation (6), we decompose the integral expression into simpler components through variable substitution. Specifically, we define two auxiliary terms: O to represent the integral part and $Q(\zeta)$ to encapsulate the exponential and algebraic expressions. This separation serves both notational clarity and computational convenience. The term $Q(\zeta)$ isolates the components that depend on the upper limit of integration ζ while O captures the structure of the full integral over the interval $[l_1, u_1]$. This transformation allows us to rewrite Equation (6) in a compact multiplicative form, as shown in Equation (7), which simplifies both analytical handling and numerical implementation. Conceptually, this step facilitates better control over the expression's complexity, making it more suitable for algorithmic computation of the Average Run Length (ARL).

Now, we examine converting the Equation (6) by setting new variables as

$$O=\int_{L_1}^{U_1} I(s)\exp\left(\frac{-s}{\nu(\lambda_1\lambda_2+\kappa_1\lambda_2+\lambda_1\kappa_2+\kappa_1\kappa_2)}\right) ds \quad \text{and}$$

$$Q(\zeta)=\exp\left(\begin{array}{l} (1-\lambda_2)\zeta+(\lambda_2-\lambda_1\lambda_2-\lambda_1\kappa_2)Z_{t-1}^{(1)} \\ \dfrac{-(\kappa_1\lambda_2+\kappa_1\kappa_2)X_{t-1}}{\nu(\lambda_1\lambda_2+\kappa_1\lambda_2+\lambda_1\kappa_2+\kappa_1\kappa_2)} \end{array}\right)\exp\left(\frac{\Delta}{\nu}\right)$$

This equation can then be rewritten as

$$I(\zeta)=1+\frac{Q(\zeta)}{\nu(\lambda_1\lambda_2+\kappa_1\lambda_2+\lambda_1\kappa_2+\kappa_1\kappa_2)}O \quad (7)$$

Next, the variable O is considered.

$$O=\frac{-\nu R\left[\exp\left(\frac{-U_1}{\nu R}\right)-\exp\left(\frac{-L_1}{\nu R}\right)\right]}{1+\frac{1}{\lambda_2}\exp\left(\frac{(\lambda_2-\lambda_1\lambda_2-\lambda_1\kappa_2)Z_{t-1}^{(1)}-(\kappa_1\lambda_2+\kappa_1\kappa_2)X_{t-1}}{\nu R}\right)\times\exp\left(\frac{\Delta}{\nu}\right)\left[\exp\left(\frac{-\lambda_2U_1}{\nu R}\right)-\exp\left(\frac{-\lambda_2L_1}{\nu R}\right)\right]}$$

where $R=\lambda_1\lambda_2+\kappa_1\lambda_2+\lambda_1\kappa_2+\kappa_1\kappa_2$.

By substituting constant O into Equation (7), $I(\zeta)$ becomes

$$I(\xi)=1-\exp\left(\begin{array}{l} (1-\lambda_2)\zeta+(\lambda_2-\lambda_1\lambda_2-\lambda_1\kappa_2)Z_{t-1}^{(1)} \\ \dfrac{-(\kappa_1\lambda_2+\kappa_1\kappa_2)X_{t-1}}{\nu R} \end{array}\right)\exp\left(\frac{\Delta}{\nu}\right) \times\frac{\lambda_2\left[\exp\left(\frac{-U_1}{\nu R}\right)-\exp\left(\frac{-L_1}{\nu R}\right)\right]}{\left\{\begin{array}{l}\lambda_2+\exp\left(\frac{(\lambda_2-\lambda_1\lambda_2-\lambda_1\kappa_2)Z_{t-1}^{(1)}-(\kappa_1\lambda_2+\kappa_1\kappa_2)X_{t-1}}{\nu R}\right) \\ \times\exp\left(\frac{\Delta}{\nu}\right)\left[\exp\left(\frac{-\lambda_2U_1}{\nu R}\right)-\exp\left(\frac{-\lambda_2L_1}{\nu R}\right)\right]\end{array}\right\}}$$

The explicit formula for the in-control process with the exponential parameter $\nu=\nu_0$ is as follows:

$$ARL_0\_I = 1-\exp\left(\frac{\begin{pmatrix}(1-\lambda_2)\zeta+(\lambda_2-\lambda_1\lambda_2-\lambda_1\kappa_2)Z_{t-1}^{(1)}\\-(\kappa_1\lambda_2+\kappa_1\kappa_2)X_{t-1}\end{pmatrix}}{\nu_0 R}\right)\exp\left(\frac{\Delta}{\nu_0}\right)$$
$$\times\frac{\lambda_2\left[\exp\left(\frac{-U_1}{\nu_0 R}\right)-\exp\left(\frac{-L_1}{\nu_0 R}\right)\right]}{\left\{\begin{matrix}\lambda_2+\exp\left(\frac{(\lambda_2-\lambda_1\lambda_2-\lambda_1\kappa_2)Z_{t-1}^{(1)}-(\kappa_1\lambda_2+\kappa_1\kappa_2)X_{t-1}}{\nu_0 R}\right)\\\times\exp\left(\frac{\Delta}{\nu_0}\right)\left[\exp\left(\frac{-\lambda_2 U_1}{\nu_0 R}\right)-\exp\left(\frac{-\lambda_2 L_1}{\nu_0 R}\right)\right]\end{matrix}\right\} \quad (8)$$

On the other hand, the explicit formula for the out-control process with the exponential parameter $\nu=\nu_1=\nu_0(1+\delta)$ where δ is mean shift size.

2.2.2 The IMA - DMEWMA approximate formula based on the NIE technique

The Numerical Integral Equation (NIE) technique is a powerful method for solving integral equations numerically, particularly when analytical solutions are difficult or impossible to obtain. Widely used in physics, engineering, and applied mathematics, this technique serves as a crucial tool for validating analytical formulas. In this approach, the solution is derived from the integral Equation [22] in Equation (7).

$$I(\xi)=1+\frac{1}{\lambda_1\lambda_2+\kappa_1\lambda_2+\lambda_1\kappa_2+\kappa_1\kappa_2}$$
$$\times\int_{L_1}^{U_1} I(s)\cdot f\left(\begin{matrix}s-(1-\lambda_2)\zeta-(\lambda_2-\lambda_1\lambda_2-\lambda_1\kappa_2)Z_{t-1}^{(1)}\\+(\kappa_1\lambda_2+\kappa_1\kappa_2)X_{t-1}\\-(\lambda_1\lambda_2+\kappa_1\lambda_2+\lambda_1\kappa_2+\kappa_1\kappa_2)\Delta\\(\lambda_1\lambda_2+\kappa_1\lambda_2+\lambda_1\kappa_2+\kappa_1\kappa_2)\end{matrix}\right)ds \quad (9)$$

To achieve this, the Composite Midpoint Rule is employed, systematically dividing the domain interval $[L_1,L_2]$ into m equally spaced sub-grids, ensuring precise and efficient computation.

$$\int_a^b f(u)du=\sum_{k=1}^{p} w_k f(\phi_k)$$

where $w_k=b/p$, and $\phi_k=w_k(k-0.5)$; $k=1,2,3,...,p$.

The approximate solution using the NIE technique, as presented in Equation (9), facilitates numerical evaluation, with Equation (10) summarizing the midpoint rule approximation. Thereby, the approximation of the numerical integral for the function $I_N(\zeta)$ is

$$I_N(\zeta)\approx 1+\frac{1}{\lambda_1\lambda_2+\kappa_1\lambda_2+\lambda_1\kappa_2+\kappa_1\kappa_2}$$
$$\times\sum_{k=1}^{p} w_k I(\phi_k)\cdot f\left(\begin{matrix}\phi_k-(1-\lambda_2)\zeta-(\lambda_2-\lambda_1\lambda_2-\lambda_1\kappa_2)Z_{t-1}^{(1)}\\+(\kappa_1\lambda_2+\kappa_1\kappa_2)X_{t-1}\\-(\lambda_1\lambda_2+\kappa_1\lambda_2+\lambda_1\kappa_2+\kappa_1\kappa_2)\Delta\\(\lambda_1\lambda_2+\kappa_1\lambda_2+\lambda_1\kappa_2+\kappa_1\kappa_2)\end{matrix}\right) \quad (10)$$

2.2.3 The FIMA - DMEWMA exact formula based on fredholm integral equation

Let $F(\zeta)$ be the analytical ARL used to identify shifts in the $FIMA(d,q)$ process with exponential white noise $(\varepsilon_t\sim Exp(\nu))$ running on the DMEWMA control chart when the initial value of $Z_{t-1}^{(2)}=\xi$. The exact ARL for the FIMA–DMEWMA chart is derived in Equation (11), which follows the Fredholm integral framework similar to the IMA model.

$$FI(\xi)=1-\exp\left(\frac{\begin{pmatrix}(1-\lambda_2)\zeta+(\lambda_2-\lambda_1\lambda_2-\lambda_1\kappa_2)Z_{t-1}^{(1)}\\-(\kappa_1\lambda_2+\kappa_1\kappa_2)X_{t-1}\end{pmatrix}}{\nu R}\right)\exp\left(\frac{\Omega}{\nu}\right)$$
$$\times\frac{\lambda_2\left[\exp\left(\frac{-U_2}{\nu R}\right)-\exp\left(\frac{-L_2}{\nu R}\right)\right]}{\left\{\begin{matrix}\lambda_2+\exp\left(\frac{(\lambda_2-\lambda_1\lambda_2-\lambda_1\kappa_2)Z_{t-1}^{(1)}-(\kappa_1\lambda_2+\kappa_1\kappa_2)X_{t-1}}{\nu R}\right)\\\times\exp\left(\frac{\Omega}{\nu}\right)\left[\exp\left(\frac{-\lambda_2 U_2}{\nu R}\right)-\exp\left(\frac{-\lambda_2 L_2}{\nu R}\right)\right]\end{matrix}\right\} \quad (11)$$

Follow the same steps as for the IMA process calculation to get the Equation (12).

The explicit formula for the in-control process with the exponential parameter $\nu = \nu_0$ is as follows:

$$FI(\xi) = 1 - \exp\left(\frac{\begin{pmatrix} (1-\lambda_2)\zeta + (\lambda_2 - \lambda_1\lambda_2 - \lambda_1\kappa_2) Z_{t-1}^{(1)} \\ -(\kappa_1\lambda_2 + \kappa_1\kappa_2) X_{t-1} \end{pmatrix}}{\nu_0 R} \right) \exp\left(\frac{\Omega}{\nu_0} \right) \times \frac{\lambda_2 \left[\exp\left(\frac{-U_2}{\nu_0 R} \right) - \exp\left(\frac{-L_2}{\nu_0 R} \right) \right]}{\left\{ \begin{matrix} \lambda_2 + \exp\left(\frac{(\lambda_2 - \lambda_1\lambda_2 - \lambda_1\kappa_2) Z_{t-1}^{(1)} - (\kappa_1\lambda_2 + \kappa_1\kappa_2) X_{t-1}}{\nu_0 R} \right) \\ \times \exp\left(\frac{\Omega}{\nu_0} \right) \left[\exp\left(\frac{-\lambda_2 U_2}{\nu_0 R} \right) - \exp\left(\frac{-\lambda_2 L_2}{\nu_0 R} \right) \right] \end{matrix} \right\} \quad (12)$$

On the other hand, the explicit formula for the out-control process with the exponential parameter $\nu = \nu_1 = \nu_0(1+\delta)$ where δ is mean shift size.

2.2.4 The FIMA - DMEWMA approximate formula based on the NIE technique

In the FIMA model, when dealing with exponential white noise, the function $FI_N(\zeta)$ is evaluated using the numerical integral equation technique with the Composite Midpoint Rule to approximate the ARL on the DMEWMA control chart**.** Similar to Equation (8), the weights assigned to the start and end points are $w_k = b/p,\ \phi_k = w_k(k-0.5);\ k = 1,2,3,...,p.$

Ultimately, the numerical integral approximation for the function $FI_N(\zeta)$ is given by:

$$FI_N(\zeta) \approx 1 + \frac{1}{\lambda_1\lambda_2 + \kappa_1\lambda_2 + \lambda_1\kappa_2 + \kappa_1\kappa_2} \times \sum_{k=1}^{p} w_k I(\phi_k) \cdot f \left(\begin{matrix} \phi_k - (1-\lambda_2)\zeta - (\lambda_2 - \lambda_1\lambda_2 - \lambda_1\kappa_2) Z_{t-1}^{(1)} \\ + (\kappa_1\lambda_2 + \kappa_1\kappa_2) X_{t-1} \\ \frac{-(\lambda_1\lambda_2 + \kappa_1\lambda_2 + \lambda_1\kappa_2 + \kappa_1\kappa_2)\Omega}{(\lambda_1\lambda_2 + \kappa_1\lambda_2 + \lambda_1\kappa_2 + \kappa_1\kappa_2)} \end{matrix} \right) \quad (13)$$

3 Results and Discussion

3.1 *Establishing the control limits*

To analyze the control process, we will determine the Upper Control Limit (UCL) using the exact formula. This will help us observe the direction of the control limit for each process. The process mean is set at $\nu_0 = 1$ and the initial ARL_0 is predefined as 370. The control limits can be adjusted based on different combinations of λ_1, λ_2 and K_1,K_2 to align with the predefined ARL_0 values. For the DMEWMA control chart, the parameter sets chosen for (λ_1, λ_2) are (0.05,0.1), (0.10,0.2), and (0.20,0.25). Similarly, for the smoothing parameters, the selected combinations for (κ_1, κ_2) are selected as (0.2,0.5), (0.5,0.7), (1,2), and (3,5). Additionally, the parameters θ_1 and θ_2 are defined as 0.1 and 0.2, respectively. For the IMA process, the initial conditions are set to $I_{t-1}, I_{t-2}, I_{t-3}, ..., I_{t-d} = 1$, while for the FIMA process, the initial conditions are $FI_{t-1}, FI_{t-2}, FI_{t-3}, ..., FI_{t-d} = 1$.

3.1.1 Construction of the control limits for IMA

Table 2 summarizes the results from two analytical perspectives. Firstly, with respect to the constants (K_1,K_2), it was found that the DMEWMA control chart configured with q = 1, K_1 = 0.2 and K_2 = 0.5 produced an upper control limit (UCL) of 0.01389 for both d = 1 and d = 2. An increase in the values of (K_1,K_2) the corresponding led to higher UCLs. Secondly, when considering the effect of the smoothing parameter, λ_1, λ_2 it was similarly observed that larger values of (λ_1, λ_2) resulted in increased UCLs. Nonetheless, within each configuration of κ_1, κ_2, the variation in the UCL due to changes in λ_1, λ_2 remained relatively small. For example, for (K_1,K_2) = (1,2), the UCL values obtained were 0.85086, 0.898933, and 0.968456, respectively. This trend is consistently observed in the case where q = 2, as well.

3.1.2 Construction of the control limits for FIMA

The results presented in Table 3 align with those observed in Table 1. Specifically, as the values of K_1,K_2 and λ_1, λ_2 increase, the upper control limit (UCL) also increases. However, a key distinction arises when comparing the *FIMA*(d,1) and *FIMA*(d,2) models. In the case of *FIMA*(d,1), the UCL varies with different values of d, indicating a sensitivity to the differencing order. Conversely, for FIMA(d,2), variations in d have no observable effect on the UCL, suggesting robustness with respect to this parameter.

Table 2: Upper control limit values for the DMEWMA control chart with $ARL_0 = 370$ on *IMA*(*d*,*q*) process.

λ		K_1,K_2	*IMA*(*d*,1)		*IMA*(*d*,2)	
λ_1	λ_2		***d* = 1**	***d* = 2**	***d* = 1**	***d* = 2**
0.05	0.1	0.2,0.5	0.013890	0.013890	0.017065	0.017065
		0.5,0.7	0.139000	0.139000	0.170464	0.170464
		1,2	0.850860	0.850860	1.043895	1.043895
		3,5	6.356550	6.356550	7.800439	7.800439
0.1	0.2	0.2,0.5	0.025894	0.025894	0.031750	0.031750
		0.5,0.7	0.148545	0.148545	0.182615	0.182615
		1,2	0.898933	0.898933	1.107440	1.107440
		3,5	6.644260	6.644260	8.193140	8.193140
0.2	0.25	0.2,0.5	0.042837	0.042837	0.052551	0.052551
		0.5,0.7	0.179410	0.179410	0.220860	0.220860
		1,2	0.968456	0.968456	1.195257	1.195257
		3,5	6.897273	6.897273	8.525740	8.525740

Table 3: Upper control limit values for the DMEWMA control chart with $ARL_0 = 370$ on the *FIMA*(*d*,*q*) process.

λ		K_1,K_2	*FIMA*(*d*,1)		*FIMA*(*d*,2)	
λ_1	λ_2		***d* = 0.25**	***d* = 0.50**	***d* = 0.25**	***d* = 0.50**
0.05	0.1	0.2,0.5	0.022220	0.016651	0.017065	0.017065
		0.5,0.7	0.221347	0.166366	0.170464	0.170464
		1,2	1.356379	1.018748	1.043895	1.043895
		3,5	10.13926	7.612310	7.800450	7.800450
0.1	0.2	0.2,0.5	0.041215	0.030987	0.031750	0.031750
		0.5,0.7	0.238070	0.178169	0.182615	0.182615
		1,2	1.448771	1.080178	1.107440	1.107440
		3,5	10.73531	7.990450	8.193140	8.193140
0.2	0.25	0.2,0.5	0.068271	0.051286	0.052551	0.052551
		0.5,0.7	0.288577	0.215444	0.220860	0.220860
		1,2	1.568405	1.165555	1.195257	1.195257
		3,5	11.21660	8.312170	8.525740	8.525740

3.2 *Experimental results*

The experimental results presented in this study are obtained using a simulation method with 1,000 iterations conducted in the Mathematica program. The process is divided into two main steps: first, verifying the accuracy of the proposed formula by ensuring it aligns with the NIE technique; second, comparing the performance of the DMEWMA control chart with the MEWMA chart when the process mean shifts. Specifically, the mean shift values are set at δ = 0.01, 0.02, 0.05, 0.10, 0.20, 0.50, 1.00 and 2.00.

3.2.1 Performance of the control charts

To evaluate performance in terms of ARL_1, we compare the results obtained using the proposed formula with those from the NIE technique. A smaller ARL_1 value indicates better statistical performance. Additionally, the proposed formula is assessed against the NIE technique based on computation time (in seconds) and percentage accuracy by

$$\%Acc = 100 - \left| \frac{ARL(\zeta) - ARL_N(\zeta)}{ARL(\zeta)} \right| \times 100\%$$

where $ARL(\zeta)$ is the ARL values obtained by using the exact formula and ARL_N is the ARL values obtained by using the NIE technique. Strong agreement between the two approaches is demonstrated by a percentage value close to 100%, which shows that the ARL_1 derived from the proposed formula substantially resembles the outcome from the numerical integration equation (NIE) technique.

To evaluate the computational efficiency of the proposed analytical solution, we compared its performance against the NIE technique under various parameter settings. The analytical method consistently yielded accurate ARL_1 values (with 100% agreement to NIE) while requiring computation times of less than

0.001 seconds in all cases. In contrast, the NIE approach took several seconds to complete, and its runtime increased with the complexity of the parameter values.

These findings highlight a key practical advantage of the proposed method: it offers both high accuracy and substantial reductions in computational cost, making it suitable for use in real-time monitoring environments or large-scale simulations.

Tables 4 and 5 present the results of a comparative analysis between the proposed method and the NIE technique in terms of ARL_1 values, computation time, and accuracy percentage applied to the *IMA*(d,q) and *FIMA*(d,q) models, respectively. The findings demonstrate that the out-of-control ARL values computed using the formula-based method closely approximate those obtained via the NIE technique, as confirmed by the percentage accuracy metric. Notably, the percentage accuracy is 100% across all cases. Both methods exhibit high sensitivity in detecting process shifts. However, the formula method demonstrates a clear advantage in computational efficiency, yielding results almost instantaneously. In contrast, the NIE technique requires significantly more computation time, which increases with the complexity of the conditions. Overall, the comparison affirms the strong agreement between the two approaches and highlights the high accuracy and practical efficiency of the proposed formula-based method.

Table 4: Comparison of the accuracy of the exact formula and NIE technique for the *IMA*(*1*,*q*) process with $\theta = 0.1$.

Coefficients			δ	0.00	0.01	0.05	0.10	0.50	1.00
λ_1, λ_2	K_1,K_2	q		ARL_0 (time)	ARL_1 (time)	ARL_1 (time)	ARL_1 (time)	ARL_1 (time)	ARL_1 (time)
0.05,0.1	0.2,0.1	1	Exact	369.9649893 (<0.001)	331.5503537 (<0.001)	220.3416822 (<0.001)	139.8602541 (<0.001)	13.2122151 (<0.001)	3.3397219 (<0.001)
			NIE	369.9649865 (6.58)	331.5503539 (7.21)	220.3416821 (7.74)	139.8602541 (8.03)	13.2122151 (8.87)	3.3397212 (9.28)
			%Acc	100	100	100	100	100	100
		2	Exact	369.9869431 (<0.001)	332.7873170 (<0.001)	223.9747898 (<0.001)	143.9567985 (<0.001)	14.2667338 (<0.001)	3.6220199 (<0.001)
			NIE	369.9869027 (10.13)	332.7873171 (10.79)	223.9747185 (11.06)	143.9567938 (12.60)	14.2667339 (12.44)	3.6220117 (13.91)
			%Acc	100	100	100	100	100	100
	1,2	1	Exact	370.17523440 (<0.001)	56.06197828 (<0.001)	13.28776187 (<0.001)	7.12077396 (<0.001)	2.10075377 (<0.001)	1.50608020 (<0.001)
			NIE	370.17523529 (6.29)	56.06162084 (7.02)	13.28792650 (8.67)	7.12079844 (9.27)	2.10079925 (10.81)	1.59749579 (10.96)
			%Acc	100	100	100	100	100	100
		2	Exact	369.98480738 (<0.001)	59.69587655 (<0.001)	14.26983668 (<0.001)	7.64976073 (<0.001)	2.23112934 (<0.001)	1.57805497 (<0.001)
			NIE	369.98481185 (12.37)	59.69593759 (12.55)	14.26983630 (13.74)	7.64976295 (14.81)	2.23112923 (15.48)	1.57803860 (16.77)
			%Acc	100	100	100	100	100	100
0.2,0.25	0.5,0.7	1	Exact	370.05815532 (<0.001)	90.76015149 (<0.001)	22.20839354 (<0.001)	11.29054195 (<0.001)	2.48898928 (<0.001)	1.58354985 (<0.001)
			NIE	370.05815376 (8.62)	90.76015227 (9.19)	22.20833740 (10.48)	11.29051880 (11.92)	2.48898997 (11.99)	1.58354118 (12.74)
			%Acc	100	100	100	100	100	100
		2	Exact	369.98225985 (<0.001)	95.84630260 (<0.001)	23.81170410 (<0.001)	12.14487326 (<0.001)	2.66183562 (<0.001)	1.66566662 (<0.001)
			NIE	369.98225983 (8.89)	95.84630898 (9.39)	23.81170987 (10.93)	12.14489879 (12.75)	2.66183398 (12.79)	1.66566119 (14.83)
			%Acc	100	100	100	100	100	100
	3,5	1	Exact	370.00774435 (<0.001)	43.18049036 (<0.001)	10.24616089 (<0.001)	5.65831863 (<0.001)	1.91262908 (<0.001)	1.44617959 (<0.001)
			NIE	370.00774436 (10.28)	43.18049299 (11.59)	10.24616909 (11.73)	5.65831828 (12.58)	1.91262928 (13.66)	1.44617039 (13.84)
			%Acc	100	100	100	100	100	100
		2	Exact	369.99238761 (<0.001)	46.54677493 (<0.001)	11.10325344 (<0.001)	6.11906555 (<0.001)	2.03137437 (<0.001)	1.51460586 (<0.001)
			NIE	369.99238738 (10.78)	46.54677495 (11.39)	11.10325457 (11.90)	6.11906551 (13.04)	2.03137435 (13.68)	1.51460544 (15.03)
			%Acc	100	100	100	100	100	100

Table 5: Comparison of the accuracy of the exact formula and NIE technique for the *FIMA*(*0.25*,*q*) process with $\theta_1 = 0.1, \theta_2 = 0.2$.

Coefficients			δ	0.00	0.01	0.05	0.10	0.50	1.00
λ_1, λ_2	K_1,K_2	*q*		*ARL₀ (time)*	*ARL₁ (time)*	*ARL₁ (time)*	*ARL₁ (time)*	*ARL₁ (time)*	*ARL₁(time)*
0.05,0.1	0.2,0.1	1	Exact	369.93724008 (<0.001)	334.30936034 (<0.001)	228.69997057 (<0.001)	149.41166837 (<0.001)	15.77569259 (<0.001)	4.03967393 (<0.001)
			NIE	369.93724039 (5.98)	334.30934567 (6.21)	228.69997098 (7.49)	149.41166568 (7.99)	15.77569457 (8.36)	4.03967348 (9.32)
			%Acc	100	100	100	100	100	100
		2	Exact	369.98694311 (<0.001)	332.78731701 (<0.001)	223.97478989 (<0.001)	143.95679853 (<0.001)	14.26673387 (<0.001)	3.62201997 (<0.001)
			NIE	369.98694337 (6.44)	332.78731702 (7.27)	223.97432530 (7.85)	143.95679835 (8.37)	14.26645369 (9.26)	3.62201578 (10.33)
			%Acc	100	100	100	100	100	100
	1,2	1	Exact	370.03812943 (<0.001)	65.15123596 (<0.001)	15.77372525 (<0.001)	8.46150646 (<0.001)	2.43208072 (<0.001)	1.68981286 (<0.001)
			NIE	370.03578500 (6.84)	65.15123546 (7.25)	15.77372354 (8.21)	8.46157575 (9.11)	2.43208089 (10.10)	1.68981288 (11.34)
			%Acc	100	100	100	100	100	100
		2	Exact	369.98480738 (<0.001)	59.69587655 (<0.001)	14.26983668 (<0.001)	7.64976073 (<0.001)	2.23112934 (<0.001)	1.57805497 (<0.001)
			NIE	369.98484486 (8.65)	59.69587038 (9.23)	14.26983347 (9.87)	7.64976798 (10.34)	2.23117978 (11.27)	1.57805978 (11.67)
			%Acc	100	100	100	100	100	100
0.2,0.25	0.5,0.7	1	Exact	369.98289432 (<0.001)	103.24401424 (<0.001)	26.22293766 (<0.001)	13.43726552 (<0.001)	2.92659543 (<0.001)	1.79283915 (<0.001)
			NIE	369.98289424 (8.24)	103.24401430 (9.53)	26.22293457 (9.56)	13.43726436 (10.22)	2.92659058 (11.53)	1.79284577 (12.12)
			%Acc	100	100	100	100	100	100
		2	Exact	369.98225985 (<0.001)	95.84630260 (<0.001)	23.81170410 (<0.001)	12.14487326 (<0.001)	2.66183562 (<0.001)	1.66566662 (<0.001)
			NIE	369.98225985 (8.67)	95.84630277 (9.43)	23.81170498 (10.36)	12.14487329 (11.28)	2.66183563 (11.82)	1.66566648 (12.88)
			%Acc	100	100	100	100	100	100
	3,5	1	Exact	369.92824153 (<0.001)	51.85960425 (<0.001)	12.48076333 (<0.001)	6.85986400 (<0.001)	2.22157480 (<0.001)	1.62446498 (<0.001)
			NIE	369.92824164 (8.71)	51.85960429 (9.52)	12.48076330 (10.46)	6.85986346 (11.62)	2.22157479 (12.03)	1.62446498 (12.60)
			%Acc	100	100	100	100	100	100
		2	Exact	369.99238761 (<0.001)	46.54677493 (<0.001)	11.10325344 (<0.001)	6.11906555 (<0.001)	2.03137437 (<0.001)	1.51460586 (<0.001)
			NIE	369.99238723 (9.46)	46.54677493 (9.87)	11.10325335 (10.34)	6.11906558 (11.45)	2.03137436 (12.04)	1.51460589 (13.98)
			%Acc	100	100	100	100	100	100

3.2.2 Compare the control charts

Previous studies have investigated the effectiveness of EWMA and MEWMA control charts under fractionally integrated processes. Notably, Phanthuna and Areepong [19] compared these methods and concluded that MEWMA provides better detection sensitivity than classical EWMA, particularly in the presence of long-memory structures. Their work, which used IMA and FIMA models, demonstrated the limitations of EWMA when applied to autocorrelated data with fractional differencing.

Building upon these findings, the present study introduces the DMEWMA control chart as a further enhancement. By incorporating a second smoothing parameter, DMEWMA outperforms MEWMA in terms of ARL_1 values across a broader range of shift magnitudes. In particular, the DMEWMA chart achieves superior performance not only in early detection of small shifts but also maintains stability and robustness under moderate and large process changes. This progression—from EWMA to MEWMA and now to DMEWMA—illustrates a natural evolution in control chart design tailored for complex time series data.

The performance of the DMEWMA and MEWMA control charts is compared across various values of λ_1, λ_2 with the ARL for the DMEWMA control chart calculated using the proposed exact formula. To evaluate the overall performance, the relative mean index (RMI) [23] and the average extra quadratic loss (AEQL) [24] are utilized. These metrics are calculated using the formulas with

$$RMI = \frac{1}{v}\sum_{u=1}^{v}\frac{ARL_1(r_u) - ARL_1^{\min}(r_u)}{ARL_1^{\min}(r_u)}, \text{ and,}$$

$$AEQL = \frac{1}{\Lambda}\sum_{\delta_i=\delta_{\min}}^{\delta_{\max}}\left(\delta_i^2 \times ARL(\delta_i)\right)$$

where v is number of shifts size considered, $ARL_1(r_u)$ and $ARL_1^{\min}(r_u)$ are the ARL_1 values and the smallest ARL_1 values, receptively. For the δ_i represents the value of the shift change for order i in the process, and Λ is the sum of shift change values from $\delta_{\min} = 0.01$ to $\delta_{\max} = 2$. The control chart that achieves the lowest values for both the RMI and the AEQL is considered the most effective tool for detecting changes in the process.

Tables 8 and 9 present a performance comparison between the MEWMA and DMEWMA control charts under the *IMA*(1,1) and *FIMA*(0.5,1) models, respectively, across varying parameter settings. For each chart, the smoothing parameter λ is defined as follows: for the MEWMA chart, $\lambda = \lambda_1$ with the constant $\kappa = \kappa_1$ also specified to capture sensitivity to process changes. Additionally, various coefficient parameters are considered while maintaining a constant in-control Average Run Length (ARL_1) of 370.

To evaluate the performance of the control charts, three key metrics are compared: the out-of-control Average Run Length (ARL_1), the RMI, and the AEQL. The findings from both tables exhibit consistent trends:

ARL_1: The MEWMA control chart demonstrates superior performance under small to moderate shifts when both λ and κ are small (e.g., 0.05, 0.1). However, as λ increases to 0.1 and 0.2, the DMEWMA control chart outperforms MEWMA, particularly when $(\kappa_1, \kappa_2) = (0.2, 0.5)$. In scenarios involving larger values of κ, the DMEWMA chart exhibits more effective performance.

RMI: The MEWMA control chart achieves favorable RMI values only when κ_1, κ_2 are at their smallest values (0.2, 0.5), regardless of the value of λ. In all other configurations, the DMEWMA control chart yields superior RMI performance.

AEQL: The DMEWMA control chart shows improved performance across nearly all conditions, with the exception of cases where $(\lambda_1, \lambda_2) = (0.05, 0.1)$ and $(\kappa_1, \kappa_2) = (0.2, 0.5)$, in which the MEWMA control chart slightly outperforms. Figure 3 illustrates the Relative Median Index (RMI) across different parameter settings, highlighting the superior performance of the DMEWMA chart compared to MEWMA in both IMA and FIMA models. Similarly, Figure 4 presents the Average Expected Quadratic Loss (AEQL), reinforcing the observation that the DMEWMA chart consistently yields lower loss values under all conditions. Both Figures 3 and 4 are graphical representations derived from the results shown in Tables 8 and 9, respectively, which summarize the comparative performance metrics of the control charts under various shift conditions and smoothing parameter configurations.

In summary, based on the combined evaluation of ARL_1, RMI, and AEQL, the DMEWMA control chart demonstrates robust and consistent performance when κ_1, κ_2 assuming medium to high values and λ_1, λ_2 are set at a moderate level.

3.3 *Applications*

3.3.1 Real data represented by IMA process

The first dataset utilized in this study comprises daily energy absolute (EA) PCL data from Thailand, spanning the period from January 1 to March 20, 2025, totaling 55 observations, whose data characteristics are shown in Figure 1. The data were retrieved from Investing.com (https://th.investing.com/equities/energy-historical-data), accessed on March 21, 2025. To model the underlying structure of the series, the *IMA*(d,q) model was employed, and parameter estimation was conducted using SPSS.

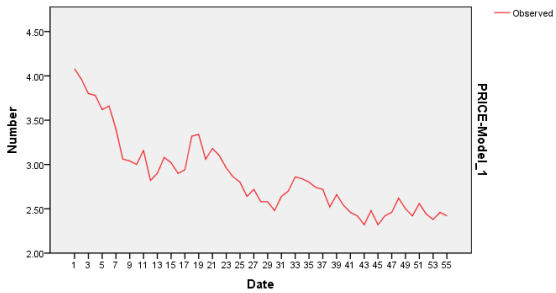

Figure 1: The characteristics of the PCL data.

The adequacy of the model residuals was evaluated via the Kolmogorov–Smirnov test to assess their conformity with an exponential distribution, as shown in Table 6.

Table 6: Kolmogorov–Smirnov test results for exponential distribution assumption for PCL data.

Model	Exponential Parameter	P-value
IMA(1,1)	0.1208	0.402

The analysis revealed that the data are appropriately characterized by an $IMA(1,1)$ process, specified as:

$$I_t = -0.030 + \varepsilon_t + 0.149\varepsilon_{t-1} + I_{t-1}; \varepsilon_t \sim Exp(0.1208)$$

This suggests that the series exhibits characteristics consistent with a first-order integrated moving average process with exponentially distributed innovations.

3.3.2 Real data represented by FIMA process

The second dataset analyzed in this study consists of monthly stock data for PTT Public Company Limited (PTT PCL) in Thailand, covering the period from April 2021 to March 2025, with a total of 48 observations whose data characteristics are shown in Figure 2. These data were sourced from Investing.com (https://th.investing.com/equities/ptt-historical-data) and accessed on March 21, 2025. To capture the temporal dependencies within the series, the $FIMA(d,q)$ modeling approach was applied, with model fitting performed using SPSS.

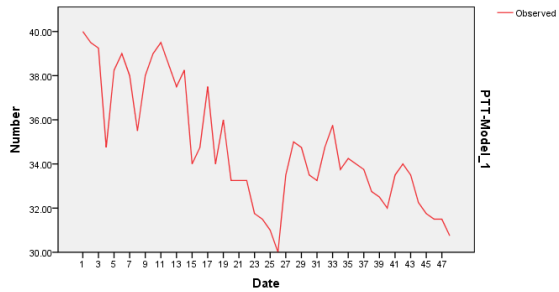

Figure 2: The characteristics of the PTT data.

The residuals from the fitted model were subjected to the Kolmogorov–Smirnov test to evaluate their goodness-of-fit to an exponential distribution, as shown in Table 7.

Table 7: Kolmogorov–Smirnov test results for exponential distribution assumption for PTT data.

Model	Exponential Parameter	P-value
FIMA(0.5,1)	1.4844	0.985

The results indicate that the series is well-represented by an *FIMA*(0.5,2) model, formally expressed as:

$$FI_t = 34.705 + \varepsilon_t + 0.7\varepsilon_{t-1} + 0.668\varepsilon_{t-2} + 0.5FI_{t-1} + 0.125FI_{t-2} + ...; \varepsilon_t \sim Exp(1.4844)$$

This outcome implies that the series demonstrates properties characteristic of a second-order fractionally integrated moving average process with innovations following an exponential distribution.

Table 8: Comparison of the performance of the DMEWMA control chart and the MEWMA control chart on the $IMA(1,1)$ process with $\theta = 0.1$.

λ_1, λ_2	K_1, K_2	0.2,0.5		0.5,0.7		1,2		3,5	
	Model	$Z_t^{(1)}$	$Z_t^{(2)}$	$Z_t^{(1)}$	$Z_t^{(2)}$	$Z_t^{(1)}$	$Z_t^{(2)}$	$Z_t^{(1)}$	$Z_t^{(2)}$
	δ	U=0.075864	0.013890	0.203459	0.139000	0.408730	0.850860	1.228420	6.356550
0.05,0.1	0.00	370.019	369.965	370.012	370.710	369.920	370.175	370.060	370.162
	0.01	**292.628**	331.550	**142.684**	166.170	82.647	**56.062**	51.982	**42.496**
	0.02	**239.197**	298.068	**87.518**	105.743	46.531	**30.623**	28.296	**22.964**
	0.05	**147.646**	220.342	**39.509**	48.870	20.175	**13.288**	12.317	**10.086**
	0.1	**82.2419**	139.860	**19.874**	24.423	10.452	**7.121**	6.661	**5.579**
	0.2	**36.6877**	64.901	**9.478**	11.288	5.453	**3.975**	3.776	**3.285**
	0.5	**9.26782**	13.212	**3.547**	3.899	2.526	**2.101**	2.050	**1.900**
	1	**3.21051**	3.340	**1.942**	2.001	1.648	**1.506**	1.493	**1.441**
	2	1.5766	**1.414**	1.346	**1.343**	1.274	**1.232**	1.231	**1.216**
	RMI	**7.281599**	11.23602	**1.73185**	2.214921	0.628242	**0.20259**	0.143449	**0**
	AEQL	**1.827231**	2.12461	**1.11747**	1.153074	0.972097	**0.905067**	0.89941	**0.87573**

Table 8: *(Continued)*

λ_1, λ_2	K_1, K_2	0.2,0.5		0.5,0.7		1,2		3,5	
	Model	$Z_t^{(1)}$	$Z_t^{(2)}$	$Z_t^{(1)}$	$Z_t^{(2)}$	$Z_t^{(1)}$	$Z_t^{(2)}$	$Z_t^{(1)}$	$Z_t^{(2)}$
	δ	U=0.075864	0.013890	0.203459	0.139000	0.408730	0.850860	1.228420	6.356550
0.1,0.2		0.084565	0.025894	0.207920	0.148545	0.413935	0.898933	1.241170	6.644260
	0.00	369.952	370.080	370.107	369.991	369.881	370.023	369.925	370.099
	0.01	**242.454**	277.111	122.853	**116.228**	77.207	**52.771**	51.404	**43.053**
	0.02	**177.702**	218.067	73.060	**68.347**	43.166	**28.729**	27.967	**23.275**
	0.05	**94.0586**	125.611	32.328	**29.933**	18.679	**12.477**	12.177	**10.217**
	0.1	**48.428**	65.870	16.297	**15.007**	9.717	**6.720**	6.591	**5.645**
	0.2	**21.3002**	27.564	7.923	**7.268**	5.121	**3.787**	3.744	**3.317**
	0.5	**5.99789**	6.469	3.134	**2.889**	2.424	**2.037**	2.039	**1.912**
	1	**2.47369**	2.306	1.812	**1.701**	1.611	**1.480**	1.489	**1.446**
	2	1.42814	**1.303**	1.307	**1.258**	1.261	**1.221**	1.229	**1.218**
	RMI	**4.436645**	5.765816	1.299677	**1.141955**	0.519745	**0.138091**	0.123576	**0**
	AEQL	1.41906	**1.415684**	1.053174	**1.001229**	0.954121	**0.892486**	0.897227	**0.878036**
0.2,0.25		0.0993	0.042837	0.218981	0.179410	0.425853	0.968456	1.267458	6.897273
	0.00	369.42	369.945	369.929	370.058	369.888	370.006	370.001	370.008
	0.01	**155.911**	184.170	94.827	**90.760**	68.401	**50.314**	50.351	**43.180**
	0.02	**97.4941**	120.451	54.158	**51.499**	37.832	**27.325**	27.366	**23.346**
	0.05	**44.2944**	56.202	23.474	**22.208**	16.339	**11.877**	11.921	**10.246**
	0.1	**21.9524**	27.411	11.957	**11.291**	8.571	**6.423**	6.465	**5.658**
	0.2	**10.0982**	11.931	6.029	**5.693**	4.600	**3.646**	3.684	**3.323**
	0.5	**3.51095**	3.649	2.617	**2.489**	2.264	**1.988**	2.018	**1.913**
	1	1.84844	**1.777**	1.643	**1.584**	1.550	**1.459**	1.480	**1.446**
	2	1.28382	**1.224**	1.254	**1.227**	1.239	**1.212**	1.226	**1.218**
	RMI	**1.900189**	2.436397	0.784214	**0.699123**	0.371961	**0.09693**	0.10542	**0.000619**
	AEQL	1.081279	**1.067963**	0.970556	**0.942509**	0.925404	**0.882465**	0.893261	**0.878128**

Table 9: Comparison of the performance of the DMEWMA control chart and the MEWMA control chart on the $FIMA(0.5,1)$ process with $\theta_1 = 0.1, \theta_2 = 0.2$.

λ_1, λ_2	K_1, K_2	0.2,0.5		0.5,0.7		1,2		3,5	
	Model	$Z_t^{(1)}$	$Z_t^{(2)}$	$Z_t^{(1)}$	$Z_t^{(2)}$	$Z_t^{(1)}$	$Z_t^{(2)}$	$Z_t^{(1)}$	$Z_t^{(2)}$
	δ	U=0.090842	0.01665	0.243194	0.16637	0.488494	1.01875	1.46813	7.61231
0.05,0.1	0.00	369.887	369.988	369.993	369.957	369.917	369.966	370.331	369.980
	0.01	**295.97**	332.643	**148.228**	171.695	86.792	**59.237**	54.899	**45.055**
	0.02	**243.993**	299.957	**91.83**	110.466	49.188	**32.505**	30.004	**24.425**
	0.05	**153.036**	223.539	**41.87**	51.657	21.442	**14.145**	13.091	**10.739**
	0.1	**86.459**	143.461	**21.184**	25.998	11.136	**7.582**	7.079	**5.933**
	0.2	**39.134**	67.662	**10.152**	12.09	5.816	**4.225**	4.006	**3.481**
	0.5	**10.051**	14.136	**3.801**	4.185	2.68	**2.215**	2.156	**1.994**
	1	**3.473**	3.586	**2.056**	2.121	1.727	**1.569**	1.554	**1.496**
	2	1.659	**1.47**	1.396	**1.392**	1.314	**1.266**	1.265	**1.247**
	RMI	**7.16454**	10.84528	**1.729432**	2.20395	0.629595	**0.203659**	0.143043	**0**
	AEQL	**1.945186**	2.231648	**1.17055**	1.208666	1.00987	**0.935732**	0.929281	**0.902774**
0.1,0.2		0.10125	0.03099	0.248895	0.17817	0.49559	1.08018	1.486276	7.99045
	0.00	370.258	369.955	369.977	370.012	369.816	369.994	369.927	370.008
	0.01	**247.505**	280.346	128.118	**121.295**	81.258	**55.982**	54.402	**45.871**
	0.02	**183.343**	222.389	76.894	**71.947**	45.72	**30.612**	29.72	**24.885**
	0.05	**98.54**	129.912	34.319	**31.761**	19.883	**13.327**	12.97	**10.936**
	0.1	**51.289**	68.93	17.384	**15.993**	10.365	**7.176**	7.019	**6.032**
	0.2	**22.791**	29.194	8.481	**7.769**	5.464	**4.033**	3.977	**3.53**
	0.5	**6.479**	6.938	3.349	**3.077**	2.571	**2.148**	2.147	**2.012**
	1	2.649	**2.45**	1.911	**1.786**	1.686	**1.541**	1.55	**1.505**
	2	1.489	**1.344**	1.351	**1.296**	1.299	**1.254**	1.263	**1.251**
	RMI	**4.362956**	5.596973	1.289985	**1.13049**	0.516187	**0.136907**	0.120389	**0**
	AEQL	1.499215	**1.482416**	1.099337	**1.041281**	0.990385	**0.92228**	0.927222	**0.906925**

Table 9: *(Continued)*

λ_1, λ_2	K_1, K_2	0.2,0.5		0.5,0.7		1,2		3,5	
	Model	$Z_t^{(1)}$	$Z_t^{(2)}$	$Z_t^{(1)}$	$Z_t^{(2)}$	$Z_t^{(1)}$	$Z_t^{(2)}$	$Z_t^{(1)}$	$Z_t^{(2)}$
	δ	U=0.090842	0.01665	0.243194	0.16637	0.488494	1.01875	1.46813	7.61231
0.2,0.25		0.11906	0.05129	0.262842	0.21544	0.51156	1.16556	1.52377	8.31217
	0.00	370.66	370.097	370.165	369.986	370.316	370.014	369.737	369.966
	0.01	**161.665**	189.13	99.536	**95.211**	72.309	**53.464**	53.519	**46.115**
	0.02	**102.074**	124.89	57.28	**54.417**	40.224	**29.158**	29.214	**25.021**
	0.05	**46.847**	58.926	24.987	**23.609**	17.444	**12.701**	12.753	**10.993**
	0.1	**23.359**	28.946	12.767	**12.037**	9.161	**6.863**	6.912	**6.06**
	0.2	**10.801**	12.681	6.447	**6.076**	4.912	**3.883**	3.927	**3.542**
	0.5	**3.756**	3.887	2.784	**2.64**	2.398	**2.096**	2.13	**2.016**
	1	1.95	**1.864**	1.723	**1.655**	1.62	**1.518**	1.543	**1.506**
	2	1.325	**1.255**	1.292	**1.26**	1.274	**1.244**	1.26	**1.251**
	RMI	**1.871726**	2.373047	0.776406	**0.688772**	0.368782	**0.094563**	0.103938	**0.000703**
	AEQL	1.128593	**1.108579**	1.008485	**0.97609**	0.958815	**0.911339**	0.923828	**0.907298**

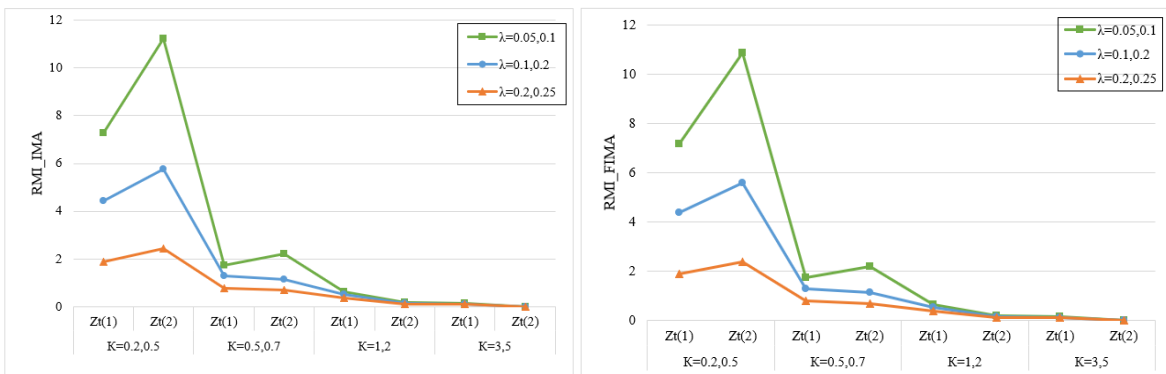

(a) (b)

Figure 3: An evaluation of the RMI for both models under differing conditions: (a) RMI corresponding to the *IMA(1,1)* model for varying K_1, K_2, (b) RMI corresponding to the *FIMA*(0.5,1) model for varying.

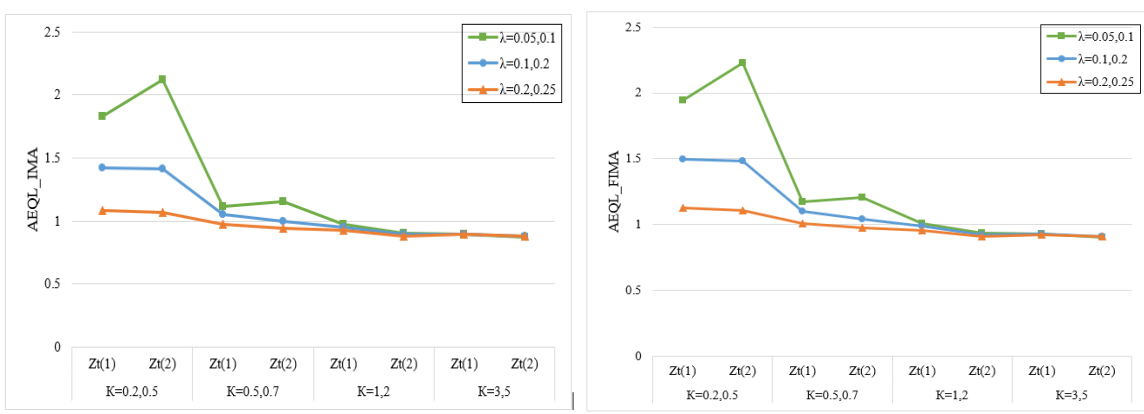

(a) (b)

Figure 4: An evaluation of the AEQL for both models under differing conditions : (a) AEQL corresponding to the *IMA(1,1)* model for varying K_1, K_2, (b) AEQL corresponding to the *FIMA(0.5,1)* model for varying.

The performance of the MEWMA and DMEWMA control charts, as presented in Tables 10 and 11, was assessed using the IMA and FIMA processes, respectively. The findings reveal that the DMEWMA chart—particularly with parameter configurations (λ_1, λ_2) set to (0.05, 0.10) and (0.10, 0.20)—consistently yields lower ARL_1 values compared to the MEWMA chart across all examined scenarios and model settings, indicating superior sensitivity in detecting out-of-control conditions. Additionally, the results from the RMI and AEQL further support the enhanced efficiency of the DMEWMA chart, as it demonstrates uniformly lower values under all conditions. These findings align closely with those obtained from the simulation study and are further illustrated by the graphical comparisons in Figures 5 and 6.

Table 10: Comparison of the performance of the control charts on the *IMA(1,1)* process modelled EA stock data.

λ_1, λ_2	K_1, K_2	1,2		λ_1, λ_2	K_1, K_2	0.5,0.7	
	Model	$Z_t^{(1)}$	$Z_t^{(2)}$		***model***	$Z_t^{(1)}$	$Z_t^{(2)}$
	δ	0.789	0.378530		δ	0.29576	0.090214
0.05,0.1	0.00	370.006	369.959	0.1,0.2	0.00	370.058	370.129
	0.01	357.296	**348.986**		0.01	362.984	**237.842**
	0.02	345.391	**329.583**		0.02	318.012	**176.392**
	0.05	313.9	**279.446**		0.05	285.651	**84.661**
	0.1	272.667	**216.584**		0.1	275.997	**50.942**
	0.2	218.138	**138.768**		0.2	142.084	**22.001**
	0.5	153.104	**52.442**		0.5	41.603	**8.852**
	1	130.901	**20.208**		1	12.718	**2.993**
	2	54.5778	**8.166**		2	4.826	**1.562**
	RMI	1.763	**0.000**		RMI	2.827	**0.000**
	AEQL	49.987378	**9.320551**		AEQL	6.467964	**1.643682**

Table 11: Comparison of the performance of the control charts on the *FIMA(0.5,2)* process modelled PTT PCL stock data.

λ_1, λ_2	K_1, K_2	1,2		λ_1, λ_2	K_1, K_2	0.5,0.7	
	Model	$Z_t^{(1)}$	$Z_t^{(2)}$		***model***	$Z_t^{(1)}$	$Z_t^{(2)}$
	δ	5.29465	4.381600		δ	7.1524	6.091234
0.05,0.1	0.00	369.825	369.799	0.2,0.25	0.00	369.729	369.930
	0.01	329.1574	**285.039**		0.01	258.384	**140.926**
	0.02	250.762	**167.334**		0.02	107.375	**62.845**
	0.05	194.0284	**105.022**		0.05	86.225	**28.014**
	0.1	78.225	**59.276**		0.1	48.004	**13.549**
	0.2	47.177	**16.883**		0.2	18.332	**5.212**
	0.5	13.72834	**8.228**		0.5	6.035	**2.892**
	1	7.58423	**4.729**		1	2.993	**1.429**
	2	3.8764	**2.012**		2	1.824	**1.287**
	RMI	0.727	**0.000**		RMI	1.410	**0.000**
	AEQL	3.726	**2.058**		AEQL	1.662	**0.969**

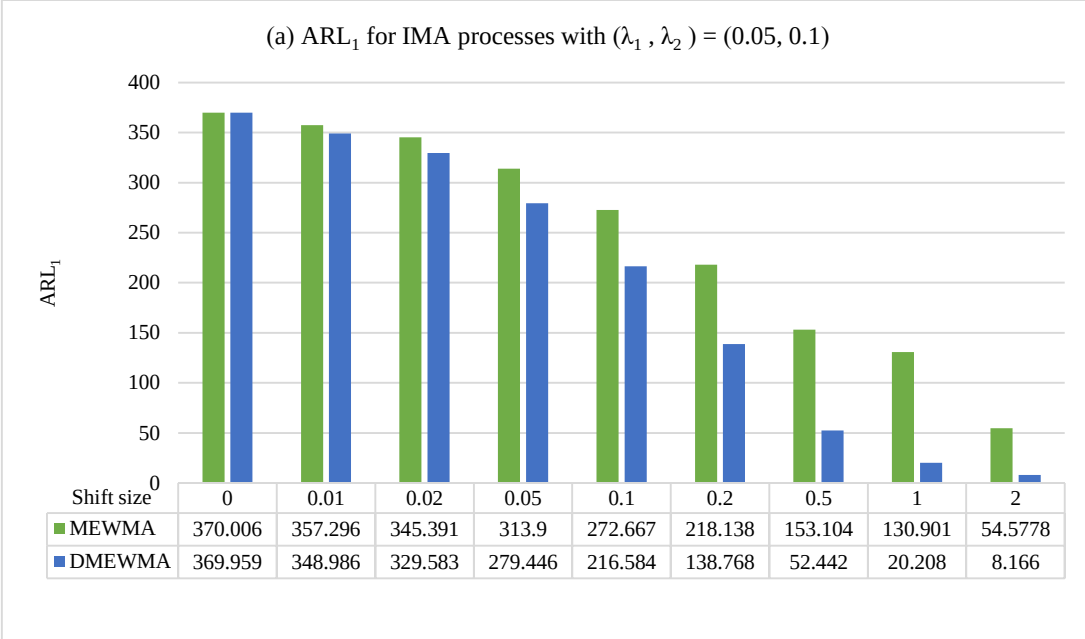

Shift size	0	0.01	0.02	0.05	0.1	0.2	0.5	1	2
MEWMA	370.006	357.296	345.391	313.9	272.667	218.138	153.104	130.901	54.5778
DMEWMA	369.959	348.986	329.583	279.446	216.584	138.768	52.442	20.208	8.166

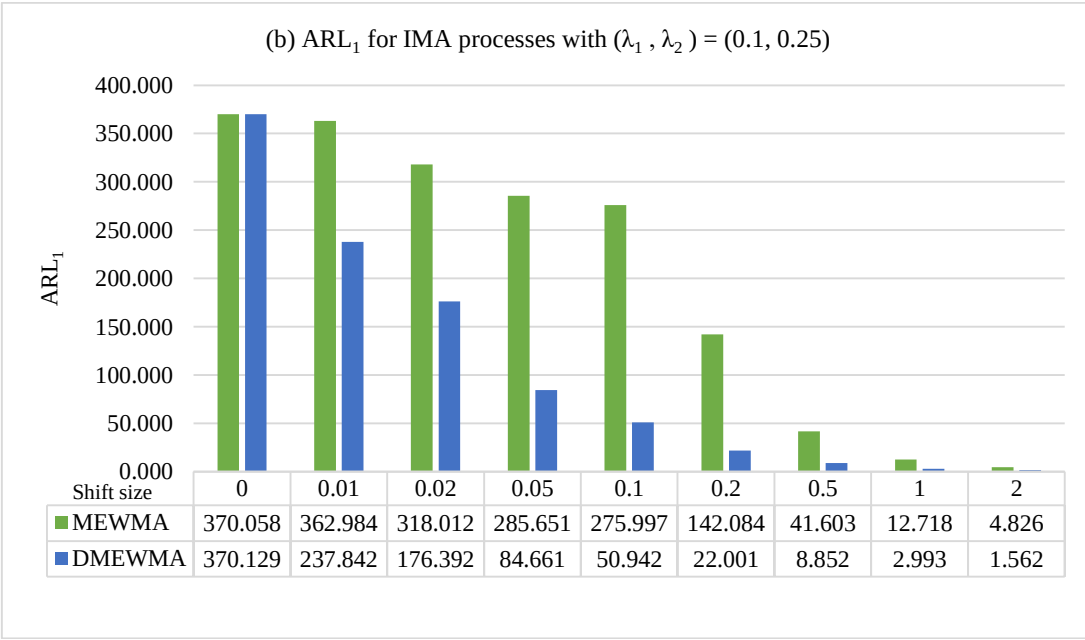

Shift size	0	0.01	0.02	0.05	0.1	0.2	0.5	1	2
MEWMA	370.058	362.984	318.012	285.651	275.997	142.084	41.603	12.718	4.826
DMEWMA	370.129	237.842	176.392	84.661	50.942	22.001	8.852	2.993	1.562

Figure 5: ARL performance of DMEWMA and MEWMA Control charts on the EA PCL stock data under different conditions : (a) $(\lambda_1, \lambda_2) = (0.05, 0.1)$ and $(\kappa_1, \kappa_2) = (1, 2)$ and (b) $(\lambda_1, \lambda_2) = (0.1, 0.2)$ and $(\kappa_1, \kappa_2) = (0.5, 0.7)$.

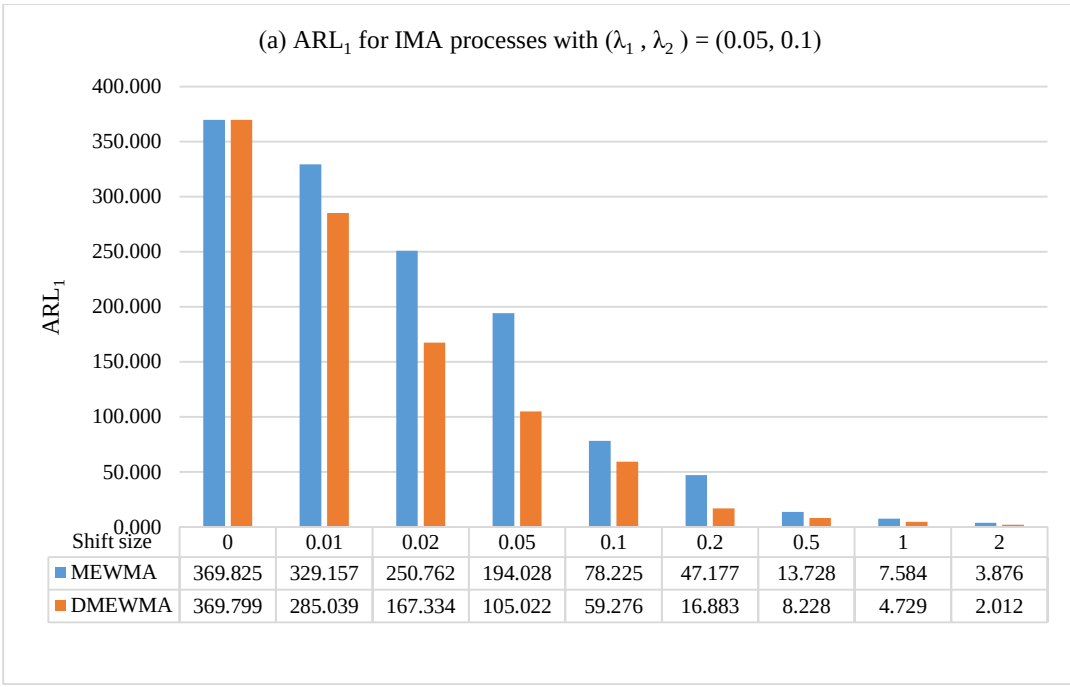

Shift size	0	0.01	0.02	0.05	0.1	0.2	0.5	1	2
MEWMA	369.825	329.157	250.762	194.028	78.225	47.177	13.728	7.584	3.876
DMEWMA	369.799	285.039	167.334	105.022	59.276	16.883	8.228	4.729	2.012

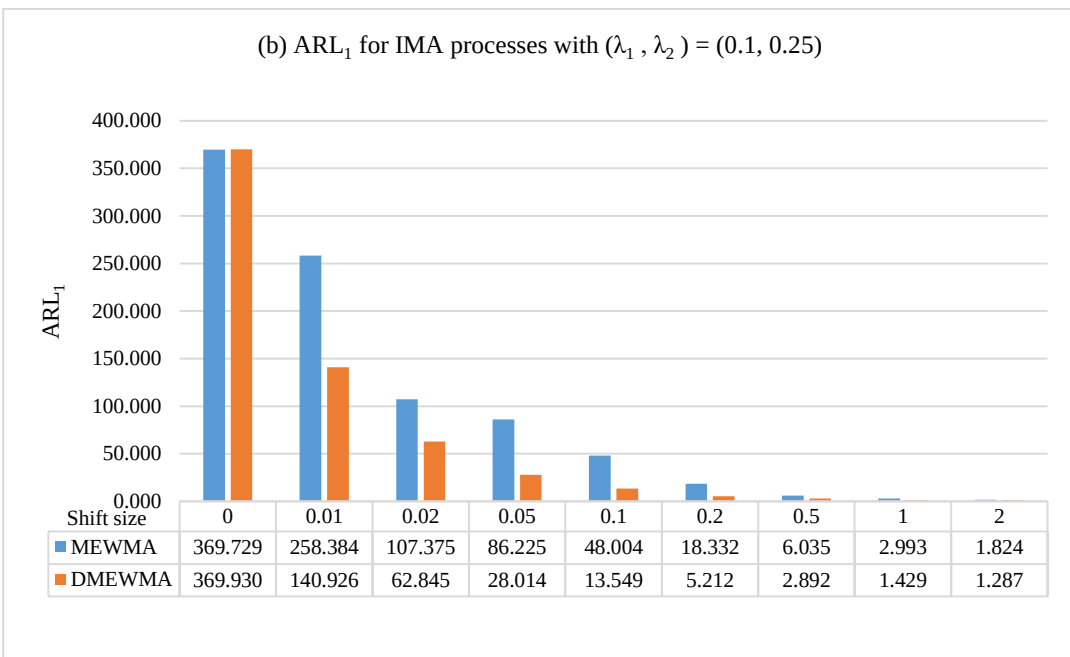

Shift size	0	0.01	0.02	0.05	0.1	0.2	0.5	1	2
MEWMA	369.729	258.384	107.375	86.225	48.004	18.332	6.035	2.993	1.824
DMEWMA	369.930	140.926	62.845	28.014	13.549	5.212	2.892	1.429	1.287

Figure 6: ARL performance of DMEWMA and MEWMA Control charts on the PTT PCL stock data under different conditions : (a) $(\lambda_1, \lambda_2) = (0.05, 0.1)$ and $(\kappa_1, \kappa_2) = (1, 2)$ and (b) $(\lambda_1, \lambda_2) = (0.1, 0.2)$ and $(\kappa_1, \kappa_2) = (0.5, 0.7)$.

4 Conclusions

The objective of this study was to improve control chart performance in identifying slight to moderate changes in the process mean of autocorrelated data, particularly data produced by IMA and FIMA processes with exponential white noise. The primary contribution lies in the development and analytical evaluation of the Double Modified Exponentially Weighted Moving Average (DMEWMA) control chart, which incorporates two smoothing parameters to increase sensitivity to subtle changes. By extending previous work on the MEWMA chart, this study proposed both an exact analytical ARL formula using Fredholm integral equations and a numerical approximation via the Numerical Integral Equation (NIE) technique to evaluate the performance of the DMEWMA chart. The theoretical development was validated through extensive simulation studies. The ARL values calculated from the proposed exact formulas were nearly identical to those obtained from the NIE technique, with accuracy levels consistently reaching 100% across all cases. Moreover, the DMEWMA control chart demonstrated significantly reduced computation time, making it a more efficient alternative, particularly in settings requiring real-time process monitoring.

The performance analysis of the DMEWMA and MEWMA control charts under various process shift scenarios and smoothing parameter configurations further emphasized the advantages of the proposed method. In every case studied—both under IMA$(1,1)$ and FIMA$(0.5,1)$ processes—the DMEWMA chart produced lower ARL_1 values, indicating quicker detection of out-of-control signals. This performance advantage became more pronounced as the size of the mean shift increased. Furthermore, evaluation using Relative Median Index (RMI) and Average Expected Quadratic Loss (AEQL) confirmed that the DMEWMA control chart maintained consistently lower values than the MEWMA chart, indicating superior overall efficiency and robustness.

Real-data applications using EA PCL and PTT PCL stock data further reinforced the chart's utility. The data were fitted to appropriate IMA and FIMA models, and the Kolmogorov–Smirnov test confirmed the exponential distribution of the residuals. In both datasets, the DMEWMA chart outperformed the MEWMA chart across all shift scenarios, delivering faster detection rates and better performance metrics. These empirical findings are consistent with those obtained from the simulation studies, thereby validating the theoretical claims in practical settings.

Based on these results, the DMEWMA control chart is recommended for use in monitoring autocorrelated processes, especially where small changes need to be detected quickly and efficiently. It is particularly suitable for financial and industrial time series where long-memory behavior and non-normal residuals are present. Future research may explore its application to multivariate settings, other distributional assumptions, or adaptive parameter selection strategies to further enhance its performance in dynamic environments.

In conclusion, the DMEWMA control chart provides a theoretically sound, computationally efficient, and practically applicable solution for monitoring complex time-dependent processes, outperforming existing methods in both accuracy and responsiveness. However, its complexity requires careful parameter selection and computational considerations.

Acknowledgments

The author sincerely appreciates the editor and referees for their valuable comments and suggestions, which have significantly improved this paper. This research budget was allocated by National Science, Research and Innovation Fund (NSRF), and King Mongkut's University of Technology North Bangkok under contract no. KMUTNB-FF-68-B-08.

Author Contributions

J.N.: investigation, methodology, data analysis, writing an original draft, reviewing and editing; S.S.: data curation, reviewing and editing; Y.A.: conceptualization, research design, reviewing and editing, funding acquisition, project administration. All authors have read and agreed to the published version of the manuscript.

Conflicts of Interest

The authors declare no conflict of interest.

References

[1] W. A. Shewhart, "Quality control charts," *The Bell System Technical Journal*, vol. 5, no. 4, pp.

593–603, 1926, doi: 10.1002/j.1538-7305.1926.tb00125.x.

[2] D. C. Montgomery, *Introduction to Statistical Quality Control*, 8th ed., NJ: John Wiley & Sons, 2020.

[3] W. H. Woodall, "Controversies and contradictions in statistical process control," *Journal of Quality Technology*, vol. 32, no. 4, pp. 341–350, 2000.

[4] C. M. Borror, *The Certified Quality Engineer Handbook*, 3rd ed., WI: ASQ Quality Press, 2008.

[5] E. S. Page, "Continuous inspection schemes," *Biometrika*, vol. 41, no. 1/2, pp. 100–115, 1954, doi: 10.2307/2333009.

[6] S. W. Roberts, "Control chart tests based on geometric moving averages," *Technometrics*, vol. 42, no. 1, pp. 97–101, 2000, doi: 10.1080/00401706.2000.10485986.

[7] J. M. Lucas and M. S. Saccucci, "Exponentially weighted moving average control schemes: Properties and enhancements," *Technometrics*, vol. 32, no. 1, pp. 1–12, Feb. 1990, doi: 10.1080/00401706.1990.10484583.

[8] N. Khan, M. Aslam, and C. H. Jun, "Design of a control chart using a modified EWMA statistic," *Quality and Reliability Engineering International*, vol. 33, no. 5, pp. 1095–1104, 2017, doi: 10.1002/qre.2102.

[9] V. Alevizakos, K. Chatterjee, and C. Koukouvinos, "Modified EWMA and DEWMA control charts for process monitoring," *Communications in Statistics-Theory and Methods*, vol. 51, no. 21, pp. 7390–7412, 2022, doi: 10.1080/03610926.2021.1872642.

[10] G. Capizzi and G. Masarotto, "A general class of control charts based on two-stage monitoring schemes," *Technometrics*, vol. 45, no. 4, pp. 268–279, 2003.

[11] G. E. P. Box and G. M. Jenkins, *Time Series Analysis: Forecasting and Control*, NY: Holden-Day, 1976.

[12] S. M. Ross, *Introduction to Probability Models*, 11th ed., MA: Academic Press, 2014.

[13] D. M. Hawkins and K. D. Zamba "Numerical integration for control chart ARL estimation," *Journal of Quality Technology*, vol. 37, no. 1, pp. 56–67, 2005.

[14] K. Petcharat, S. Sukparungsee, and Y. Areepong, "Exact solution of the average run length for the cumulative sum chart for a moving average process of order q," *ScienceAsia*, vol. 41, no. 2, pp. 141–147, 2015, doi: 10.2306/scienceasia1513-1874.2015.41.141.

[15] K. Petcharat, Y. Areepong, and S. Sukparungsee, "Exact solution of average run length of EWMA chart for MA(q) processes," *Far East Journal of Mathematical Sciences (FJMS)*, vol. 2, no. 2, pp. 1–10, 2013.

[16] Y. Supharakonsakun, "Statistical design for monitoring process mean of a modified EWMA control chart based on autocorrelated data," *Walailak Journal of Science and Technology*, vol. 18, no. 12, 2021, Art. no. 19813, doi: 10.48048/wjst.2021.19813.

[17] Y. Supharakonsakun and Y. Areepong, "ARL evaluation of a DEWMA control chart for autocorrelated data: A case study on prices of major industrial commodities," *Emerging Science Journal*, vol. 7, no. 5, pp. 1771–1786, Oct. 2023, doi: 10.28991/ESJ-2023-07-05-020.

[18] J. Neammai, S. Sukparungsee, and Y. Areepong, "Explicit analytical form for the average run length of double-modified exponentially weighted moving average control charts through the MA(q) process and applications," *Symmetry*, vol. 17, no. 2, p. 238, 2025, doi: 10.3390/sym17020238.

[19] P. Phanthuna and Y. Areepong, "Detection sensitivity of a modified EWMA control chart with a time series model with fractionality and integration," *Emerging Science Journal*, vol. 6, no. 5, pp. 1005–1018, 2022, doi: 10.28991/ESJ-2022-06-05-015.

[20] L. L. Ho, F. H. Fernandes, and M. Bourguignon, "Control charts to monitor rates and proportions," *Quality and Reliability Engineering International*, vol. 35, no. 1, pp. 74–83, 2019.

[21] P. Phanthuna, Y. Areepong, and S. Sukparungsee, "Run length distribution for a modified EWMA scheme fitted with a stationary AR(p) model," *Communications in Statistics - Simulation and Computation*, pp. 1–20, 2021, doi: 10.1080/03610918.2021.1958847.

[22] G. Burova and V. M. Ryabov, "On the solution of fredholm integral equations of the first kind," *WSEAS Transactions on Mathematics*, vol. 19, pp. 699–708, 2020, doi: 10.37394/23206.2020.19.76

[23] D. Han and F. Tsung, "A reference-free cuscore chart for dynamic mean change detection and a unified framework for charting performance

comparison," *American Statistical Association*, vol. 101, pp. 368–386, 2006, doi: 10.1198/016214505000000556

[24] V. Alevizakos, K. Chatterjee, and C. Koukouvinos, "The triple exponentially weighted moving average control chart for monitoring Poisson process," *Quality and Reliability Engineering International*, vol. 38, pp. 532–549, 2023, doi: 10.1002/qre.2999.